Subharmonic resonances in high-order wave mixing in the quantized atomic motion in a one-dimensional optical lattice

J. P. Lopez, A. J. F. de Almeida, and J. W. R. Tabosa*
Departamento de Física, Universidade Federal de Pernambuco, 50670-901 Recife, PE, Brazil

(Received 11 January 2018; published 14 March 2018)

We report on the observation of subharmonic resonances in high-order wave mixing associated with the quantized vibrational levels of atoms trapped in a one-dimensional optical lattice created by two intense nearly counterpropagating coupling beams. These subharmonic resonances, occurring at $\pm 1/2$ and $\pm 1/3$ of the frequency separation between adjacent vibrational levels, are observed through phase-match angularly resolved six- and eight-wave mixing processes. We investigate how these resonances evolve with the intensity of the incident probe beam, which couples with one of the coupling beams to create anharmonic coherence gratings between adjacent vibrational levels. Our experimental results also show evidence of high-order processes associated with coherence involving nonadjacent vibrational levels. Moreover, we also demonstrate that these induced high-order coherences can be stored in the medium and the associated optical information retrieved after a controlled storage time.

DOI: 10.1103/PhysRevA.97.033821

I. INTRODUCTION

Since the first demonstration of the confinement of atoms in a periodic array of optical potential wells, called optical lattice [1,2], about two and half decades ago, these systems have been used in a great variety of experiments. Optical lattices have been demonstrated in one, two, and three dimensions [1–7] and have been employed to mimic several effects of solid-state physics [8]. Atoms tightly confined in optical lattices have their Hilbert space expanded as a direct product of the atomic internal states and the ladder of discrete external vibrational states, therefore increasing considerably the possibility for controllable light manipulation of the atomic system. Recently, our group has demonstrated the use of the external degrees of freedom of atoms, both continuous [9] and quantized atomic states [10], to store optical information associated with a probe beam. These new types of optical memories, being associated with the external atomic motion of neutral atoms, are in principle less sensitive to stray magnetic and electric fields and therefore may allow one to achieve longer storage time.

Usually, the quantized vibrational level structure of atoms in optical lattices is directly revealed either by fluorescence or probe absorption measurements, as it was first demonstrated in [1,2], respectively via the observation of spontaneous and stimulated Raman transitions between vibrational states. Although in the very early experiments four-wave mixing (FWM) has also been used to investigate and characterize atoms in optical lattices [11,12], no detailed investigation on the general high-order nonlinear interaction of light with these atomic quantized external degrees of freedom has been performed to date. It is however worth mentioning that multiphoton transitions have been observed in atoms confined in a three-dimensional (3D) optical lattice both in the FWM spectrum [12] as well as in the probe transmission spectrum [13]. These multiphoton transitions are associated with the subharmonic Raman resonances first observed by Trebino and Rahn [14] using the ground-state hyperfine levels of sodium atoms.

In this article we use the quantized atomic external degrees of freedom to demonstrate high-order wave mixing processes, specifically six-wave mixing (SWM) and eight-wave mixing (EWM) processes, leading to subharmonic resonances at integer fraction of the frequency separation between adjacent vibrational levels of cesium atoms confined in 1D optical lattice. We use an angularly resolved phase-matched technique to select a specific order of the nonlinear susceptibility $\chi^{(2n+1)}$ [15]. Moreover, we also demonstrate experimentally that these high-order interactions can be stored into the coherence between the vibrational levels in such a way that the system can remember it after some storage time. Indeed, this concept of a nonlinear optical memory based on the Zeeman high-order nonlinear susceptibility was introduced by our group in two recent publications [16,17] and used to demonstrate the manipulation of orbital angular momentum of light. Here we extend this concept for a nonlinear optical memory based now on the quantized atomic external degrees of freedom.

It is worth mentioning that the optical memory based on the recoil induced resonance (RIR) demonstrated in [9], although also relying on the continuous atomic external degrees of freedom, does not allow the storage of high-order light-atom interaction, as we will discuss later on. Furthermore, the observation of the light storage spectrum has proved to be an efficient and more sensitive way to identify coherence between nonadjacent vibrational levels, and associated with high-order interaction as also will be discussed. Finally, we point out that the observation of these high-order light-atom interactions can, in principle, be employed to generate multiphoton quantum correlations, an essential tool in any quantum protocol involving more than two nodes distributed between communication channels. Of course, exploring the external degrees of freedom of an atomic system certainly will increase the capability for developing new and more complex quantum information protocols.

*Corresponding author: tabosa@df.ufpe.br

II. EXPERIMENTAL SCHEME AND RESULTS

The observation of high-order nonlinear processes was performed using cesium atoms obtained from a MOT with an optical density of 5 and an initial temperature of approximately 300 μK. The experimental scheme is a slight modification of the one described previously in Ref. [10]. The atoms are initially prepared in the $6S_{1/2}(F=4)$ hyperfine ground state by switching off the trapping beams and the MOT magnetic quadruple field 1 ms before the switching off of the MOT repumping beam. We use three pairs of Helmholtz coils to compensate for stray magnetic fields through a microwave spectroscopy technique described in [9,18]. After this state preparation period, we turn on the two coupling beams, specified by C_1 and C_2, together with the probe beam P, according to the geometry depicted in Fig. 1(a). All the three incident beams, as well as the generated beam D, are coplanar. The angle 2θ between coupling beam (C_1) and the probe beam (P) is equal to 2°, while the angle β indicated in the figure is fixed according to the order of the process to be analyzed. For this incident beam geometry, the optical electrical-field amplitude generated by the nonlinear polarization component $P^{(2n+1)}$, associated with the nonlinear effective susceptibility $\chi^{(2n+1)}$, is given by

$$\mathscr{E}_D(\vec{r}) \propto \chi^{(2n+1)} \mathscr{E}_{C_2} \mathscr{E}_{C_1}^{n} \mathscr{E}_P^{*n} e^{i\vec{k}_D\cdot\vec{r}}, \tag{1}$$

where $\mathscr{E}_j$ represents the electric-field amplitude associated with beam j, considered as a plane wave with wave vector $\vec{k}_j$ ($j = C_1, C_2, P, D$) for an atom at position $\vec{r}$. The phase-matching condition imposes that the signal is generated with a wave vector given by $\vec{k}_D = \vec{k}_{C_2} + n(\vec{k}_{C_1} - \vec{k}_P)$ and propagates along the direction satisfying $\sin\beta = n\sin\theta$ (or $\beta = n\theta$ for small values of θ), provided all the beams have nearly the same frequency. As we can infer from the diagrams in Fig. 1(c) and Fig. 1(d), energy conservation also imposes a different frequency for the generated beam, which differs from the pump frequency by the frequency separation, Ω_v, between adjacent vibrational levels. The signal is uniquely due to the $\chi^{(2n+1)}$ nonlinear susceptibility and corresponds to $(2n+2)$-wave mixing process.

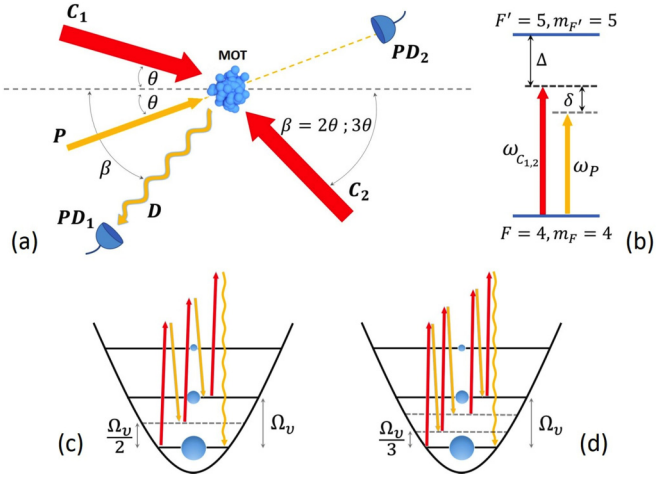

FIG. 1. (a) Simplified experimental beams configuration to observe SWM and EWM processes, corresponding respectively to the cases $\beta = 2\theta$ and $\beta = 3\theta$. PD (photodiode). (b) Partial Zeeman hyperfine levels of the cesium D_2 line interacting with the two coupling beams (C_1 and C_2), with the same frequency $\omega_{C_1} = \omega_{C_2} = \omega$, and the probe (P) beam, with frequency $\omega_P = \omega - \delta$. (c),(d) Quantized vibrational levels showing the diagrammatic interaction with the coupling and probe beams to generate the corresponding D beam, associated with the $\chi^{(5)}$ and $\chi^{(7)}$ processes.

The coupling beams have the same frequency ω which is red detuned by approximately $\Delta = 6\Gamma$ ($\Gamma/2\pi = 5.2$ MHz) from resonance of the closed transition $F=4, m_F=+4 \rightarrow F'=5, m_{F'}=+5$, while the frequency of the probe beam is detuned by δ in relation to the common frequency of the coupling beams, i.e., $\omega_P = \omega - \delta$, as indicated in the Cs partial Zeeman level scheme shown in Fig. 1(b). The coupling and the probe beams can be switched on and off by independent acousto-optic modulators, which also allow us to vary the detuning δ. All the beams having initially the same linear polarization pass through quarter waveplates in order to produce the same circular polarization states defined according to the beam propagation direction. However, different from the case of exactly counterpropagating coupling beam configuration used previously in [10], in the present case the two coupling beams propagate along slightly different directions. Thus, if we define the quantization direction along one of the coupling beams, say the C_1 beam, so this beam has a pure σ^+ circular polarization, the coupling beam C_2 will have small components of opposite σ^- circular polarization, as well as π linear polarization, owing to the small value of the angle θ. Similar consideration also applies to the polarization of the probe beam. Under these conditions, one can consider that the two coupling beams mainly will pump all the atoms in the highest magnetic sublevel $F=4, m_F=4$ and will produce the standing wave, which will provide the 1D potential wells responsible for the magnetically assisted Sisyphus cooling mechanism in the presence of a small applied transverse magnetic field, as was first demonstrated in [19]. Indeed, in our present configuration, we have observed that due to the small opposite circular polarization component present in one of the coupling beams one needs effectively a smaller transverse magnetic field to attain the same amount of cooling, an effect we are currently investigating more systematically.

The incident beams C_1, C_2, and P are left on for about 100 μs, a time long enough for the operation of the Sisyphus cooling mechanism and for the system to reach steady state. Under these conditions, if the sample longitudinal temperature T is sufficiently low, the atoms are trapped in the potential wells and the system will present a ladder of vibrational levels. The vibrational levels will have different populations when the thermal energy $k_B T$ is smaller than the vibrational energy level separation $\hbar\Omega_v$, where k_B is the Boltzmann constant and Ω_v is the classical atomic oscillating frequency in the optical potential well. In our experiment we have typically $\Omega_v \approx 150$ kHz.

First, in the upper frames of Figs. 2(b) and 2(c), we show the probe transmission spectra corresponding to the case where $\beta = 2\theta$ and $\beta = 3\theta$, respectively the geometries which correspond to the observation of SWM and EWM processes, associated to the nonlinear susceptibilities $\chi^{(5)}$ and $\chi^{(7)}$, respectively. The intensity of the coupling beams, C_1 and C_2, and the probe beam, P, are respectively equal to 70 mW/cm^2, 90 mW/cm^2, and 4 mW/cm^2. These spectra

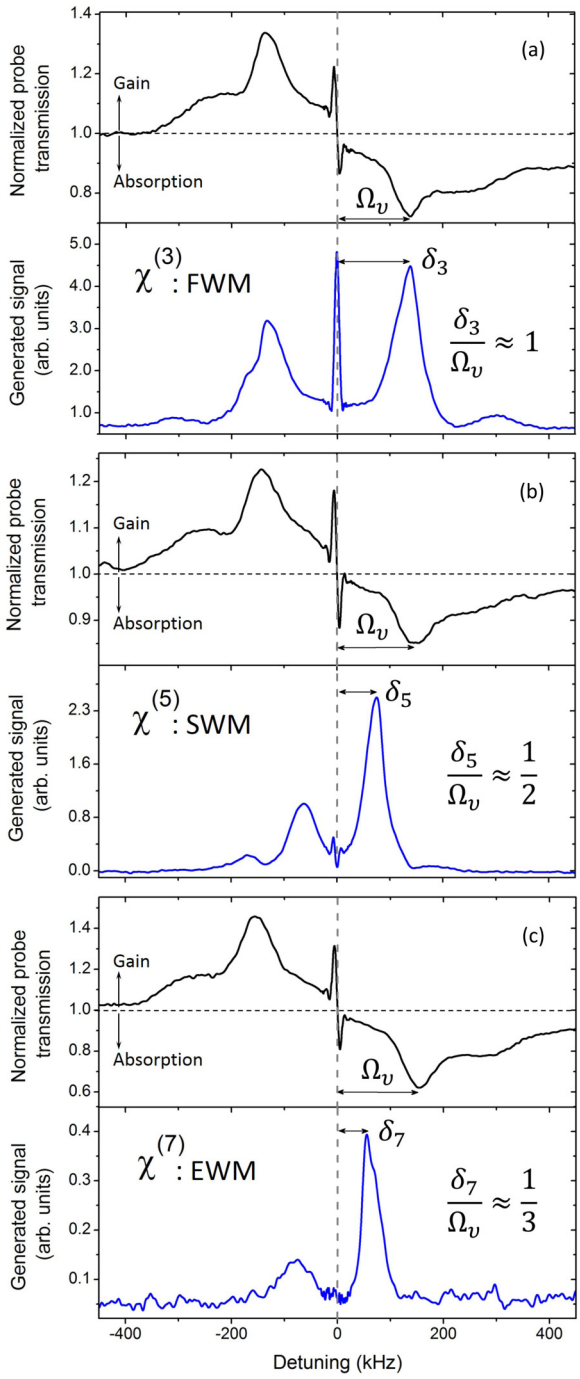

FIG. 2. (a) Probe transmission and FWM signal spectra recorded as a function of the coupling-probe detuning δ for the beam configuration shown in Fig. 1(a), for the case of $\beta = 2\theta$, but adding a weak extra counterpropagating beam to the beam C_1 in order to generate the probe conjugate FWM signal using the same vibrational level structure associated with the $\chi^{(5)}$ process. (b) Probe transmission and SWM signal spectra, corresponding to $\beta = 2\theta$; (c) probe transmission and EWM signal spectra, corresponding to $\beta = 3\theta$.

reveal clearly the Raman gain and absorption at symmetrical values of the coupling-probe detuning δ, evidencing the existence of quantized vibrational levels, having different populations, of the atoms trapped in the optical potential wells created by the two coupling beams. The narrow dispersive shaped resonance around $\delta = 0$ corresponds to the well-known RIR signal [9,20,21].

In the bottom frames of Figs. 2(b) and 2(c) we show respectively the associated SWM and EWM generated signals, recorded simultaneously with the corresponding probe transmission spectrum. The generated signal in Fig. 2(b) [Fig. 2(c)] thus corresponds to the sequential absorption of two (three) photons from the coupling beam C_1 followed by the emission of two (three) photons into the probe beam P to create a coherence grating between the two adjacent vibrational levels, which will scatter one photon from the corresponding coupling beam C_2 to generate the photon associated with the SWM (EWM) process. As depicted in the diagrammatic schemes shown in Fig. 1(c) and Fig. 1(d) these wave mixing processes are resonant when the coupling-probe detuning is respectively equal to $\delta_5 = \pm\Omega_v/2$ and $\delta_7 = \pm\Omega_v/3$, where Ω_v is the frequency separation of the pair of adjacent vibrational levels. The corresponding value of Ω_v in each case is determined by the relative position of the Raman absorption (or gain), as indicated in the upper frames of Figs. 2(b) and 2(c). The fact that the left peak associated with the $\chi^{(7)}$ signal is not exactly at a symmetric position as the right peak is attributed to propagation effects, since the frequency of the generated signal corresponding to the peak on the left experiences Raman absorption, while the one on the right experiences Raman gain, which tends to maximize its peak amplitude. We also should note the presence of symmetrically placed extra side peaks in the spectrum of the generated $\chi^{(5)}$ signal in Fig. 2(b). We attribute these peaks to the creation of Raman coherence involving more than one pair of vibrational levels, a process which is resonant for $\delta = \pm\Omega_v$ as can be seen from the diagrammatic interaction shown in Fig. 1(c). One possible reason for the smaller efficiency associated with these peaks could be attributed to the fact that such a process will only be resonant in the limit of a perfectly harmonic potential well, where the levels are equally spaced.

For the sake of comparison, we have also recorded in the bottom frame of Fig. 2(a) the signal corresponding to the usual FWM process, which is resonant for $\delta_3 = \pm\Omega_v$ and presents a very narrow peak around $\delta = 0$, associated with the RIR effect, as also described previously in [9]. To measure this signal, we added an extra weak-coupling beam, with intensity of 10 mW/cm^2 and counterpropagating to the coupling beam C_1, to the same beam configuration of Fig. 2(b) in order to generate the FWM signal using the same vibrational level structure associated with the SWM configuration. This is confirmed by the practically unchanged probe transmission spectrum shown in the upper frame of Fig. 2(a). It is worth noticing that the probe transmission and FWM spectra clearly show the overtone peaks associated with Raman resonances connecting high excited vibrational levels, as was also observed previously [10,11].

III. EXPERIMENTAL ANALYSIS AND DISCUSSIONS

In Fig. 3 we plot the peak intensity of the generated signal for different probe beam intensities for the $\chi^{(5)}$ and $\chi^{(7)}$ processes, respectively. As we should expect, the corresponding measured slopes of approximately 1.9 ± 0.3 and 2.6 ± 0.3 are consistent with the values of 2 and 3 predicted by Eq. (1). The dispersion

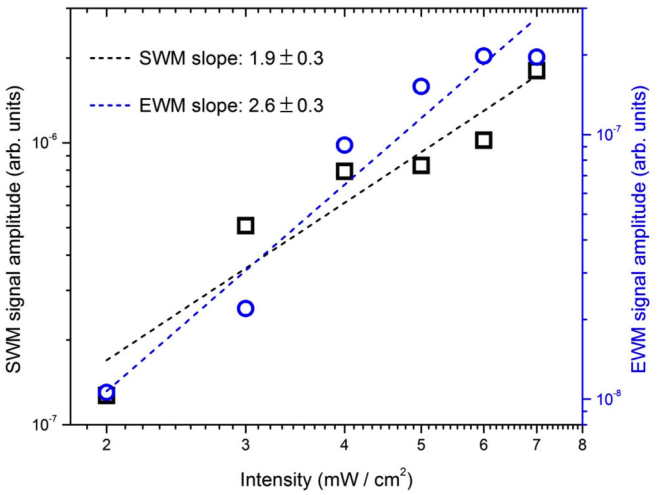

FIG. 3. Dependence of the generated signal peak amplitude with the intensity of the probe beam, for fixed intensities of the coupling beams. Circles: for the SWM ($\chi^{(5)}$) process; squares: for the EWM ($\chi^{(7)}$) process. The corresponding dotted lines correspond to linear best fitting.

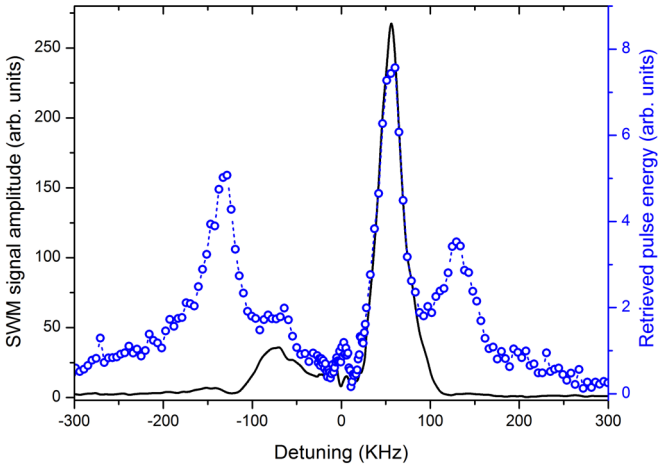

FIG. 4. Spectrum of the generated signal associated with the SWM process (continuous curve) and the corresponding light storage spectrum, obtained after a storage time of 5 μs (circled curve).

in the experimental data points could be due to the fact that the high-order processes occur for high values of the probe beam intensity, comparable to that of the coupling beams, which determine the vibrational level structure. Thus the increase in the intensity of the probe beam not only changes the efficiency of the nonlinear process, but could also affect the vibrational level structure. As described in [15], these high-order processes can be interpreted as Bragg diffraction into an anharmonic induced grating. For high intensity of the probe beam the coherence grating induced by the coupling beam C_1 and the probe beam P, which has a spatial period of $\Lambda = \frac{\lambda}{2\sin\theta}$, where λ is the optical wavelength, becomes anharmonic giving rise to high-order diffraction of the coupling beam C_2. However, one remarkable difference between these high-order spectra associated with the $\chi^{(5)}$ and $\chi^{(7)}$ processes in relation to the spectrum of the $\chi^{(3)}$ process appears around $\delta = 0$, where only the FWM process presents the signal originated by the RIR effect. As it is well known, both the probe transmission and the FWM signals around $\delta = 0$ are associated with the RIR effect and can be interpreted as the diffraction of one of the coupling beams into the atomic density grating induced by the periodic optical potential (with spatial period Λ) [9,13] created by the probe beam and the nearly copropagating coupling beam. Therefore, since this atomic density grating does not present anharmonic terms as we increase the intensity of the probe beam, the associated optical potential maintains essentially the same periodic spatial shape. Thus the Bragg condition is only satisfied for the lowest nonlinear order.

Similar to our previous demonstration of the storage of optical information via high-order nonlinear interaction using the Zeeman sublevels [17], we have also demonstrated here that these external quantized atomic level structures can be used to store high-order nonlinear light-atom interaction. Thus, in order to demonstrate the light storage in the present system, the incident beams are left on for a time of order of 100 μs, after which we switch off all the beams. The light storage signal is obtained when we switch back on only the two coupling beams and detect the retrieved signal generated by the corresponding nonlinear process. Thus, in Fig. 4 we have recorded the generated signal associated with the SWM process and the corresponding light storage signal, i.e., the retrieved pulse energy, both for the same values of intensities of the coupling beams, after a storage time of 5 μs. The storage time associated with this memory is mainly limited by the atomic motion [10]. Although the two extra symmetrically placed side peaks are barely seen in the continuously generated SWM signal, the light storage signal presents essentially the same spectral structure, but allows a better resolution for the retrieval of the signals associated with storage of coherence between the ground and higher vibrational levels as compared with the one associated with adjacent vibrational levels. A similar behavior was also observed for the signal associated with the EWM process. This indicates that the induced coherence is less sensitive to decoherence processes in the former case, where the high-order Raman resonances involve real vibrational levels, in contrast with the Raman resonances at subharmonic frequencies which are created via virtual levels. We are currently pursuing further investigation on this effect.

IV. CONCLUSIONS

In summary, we have observed subharmonic resonances associated with SWM and EWM processes employing the quantized atomic center-of-mass motion and associated with the $\chi^{(5)}$ and $\chi^{(7)}$ nonlinear susceptibilities, respectively. These subharmonic resonances are observed, respectively, at $\pm 1/2$ and $\pm 1/3$ of the frequency separation between adjacent vibrational levels, and originate from high-order coherence between these vibrational levels. High-order SWM associated with coherence involving the ground level and higher vibrational levels was also observed. Moreover, we have demonstrated that the high-order nonlinear light-atom interaction can be stored into these induced coherences, which opens up the possibility to manipulate optical information as, for instance, the one contained in the orbital angular momentum of light, as well as to generate multiphoton correlations, exploring the external degrees of freedom of atoms confined in optical lattices.

ACKNOWLEDGMENTS

We acknowledge M. Frometa for important experimental assistance. This work was supported by the Brazilian grant agencies CNPq (Conselho Nacional de Desenvolvimento Científico e Tecnológico) and FACEPE (Fundação de Amparo à Ciência e Tecnologia do Estado de Pernambuco).

[1] P. Verkerk, B. Lounis, C. Salomon, C. Cohen-Tannoudji, J.- Y. Courtois, and G. Grynberg, Phys. Rev. Lett. **68**, 3861 (1992).
[2] P. S. Jessen, C. Gerz, P. D. Lett, W. D. Phillips, S. L. Rolston, R. J. C. Spreeuw, and C. I. Westbrook, Phys. Rev. Lett. **69**, 49 (1992).
[3] G. Grynberg, B. Lounis, P. Verkerk, J.-Y. Courtois, and C. Salomon, Phys. Rev. Lett. **70**, 2249 (1993).
[4] A. Hemmerich and T. W. Hänsch, Phys. Rev. Lett. **70**, 410 (1993).
[5] A. Hemmerich, C. Zimmermann, and T. W. Hänsch, Europhys. Lett. **22**, 89 (1993).
[6] P. S. Jessen and I. H. Deutsch, Adv. At. Mol. Opt. **37**, 95 (1996).
[7] L. Guidoni and P. Verkerk, J. Opt. B: Quantum Semiclassical Opt. **1**, R23 (1999).
[8] I. Bloch, J. Dalibard, and S. Nascimbene, Rev. Mod. Phys. **80**, 885 (2008).
[9] A. J. F. de Almeida, M.-A. Maynard, C. Banerjee, D. Felinto, F. Goldfarb, and J. W. R. Tabosa, Phys. Rev. A **94**, 063834 (2016).
[10] J. P. Lopez, A. J. F. de Almeida, D. Felinto, and J. W. R. Tabosa, Opt. Lett. **42**, 4474 (2017).
[11] B. Lounis, P. Verkerk, J.-Y. Courtois, C. Salomon, and G. Grynberg, Europhys. Lett. **21**, 13 (1993).
[12] A. Hemmerich, M. Weidemuller, and T. Hänsch, Europhys. Lett. **27**, 427 (1994).
[13] A. Hemmerich, C. Zimmermann, and T. W. Hänsch, Phys. Rev. Lett. **72**, 625 (1994).
[14] R. Trebino and L. Rahn, Opt. Lett. **12**, 912 (1987).
[15] R. K. Raj, Q. F. Gao, D. Bloch, and M. Ducloy, Opt. Commun. **51**, 117 (1984).
[16] R. A. de Oliveira, G. C. Borba, W. S. Martins, S. Barreiro, D. Felinto, and J. W. R. Tabosa, Opt. Lett. **40**, 4939 (2015).
[17] G. C. Borba, D. Felinto, and J. W. R. Tabosa, J. Opt. Soc. Am. B **34**, 2528 (2017).
[18] L. Veissier, These de Doctorat, Laboratoire Kastler Brossel, Universite Pierre et Marrie Curie, 2013.
[19] B. Sheevy, S. Q. Shang, P. van der Straten, S. Hatamian, and H. Metcalf, Phys. Rev. Lett. **64**, 858 (1990).
[20] J.-Y. Courtois, G. Grynberg, B. Lounis, and P. Verkerk, Phys. Rev. Lett. **72**, 3017 (1994).
[21] D. R. Meacher, D. Boiron, H. Metcalf, C. Salomon, and G. Grynberg, Phys. Rev. A **50**, R1992(R) (1994).